American Mineralogist, Volume 68, pages 1206–1215, 1983

High-resolution silicon-29 nuclear magnetic resonance spectroscopic study of rock-forming silicates

KAREN ANN SMITH

School of Chemical Sciences
University of Illinois at Urbana-Champaign
Urbana, Illinois 61801

R. JAMES KIRKPATRICK

Department of Geology
University of Illinois at Urbana-Champaign
Urbana, Illinois 61801

ERIC OLDFIELD

School of Chemical Sciences
University of Illinois at Urbana-Champaign
Urbana, Illinois 61801

AND DONALD M. HENDERSON

Department of Geology
University of Illinois at Urbana-Champaign
Urbana, Illinois 61801

Abstract

High-resolution silicon-29 magic-angle sample-spinning NMR spectroscopic studies of a wide range of natural and synthetic silicates indicate (1) considerable overlap among the ranges of isotropic chemical shifts for crystals of different polymer types. This expands upon the work of Lippmaa *et al.* (1980), who found well-separated ranges; (2) a wide range of chemical shift anisotropies (CSA) and asymmetry parameters (η) that are related to symmetry and structure; (3) a relatively poor correlation between isotropic chemical shift and average Si–O bond length; (4) a better correlation between isotropic chemical shift and total cation-oxygen bond strength for the four oxygens of each silicon tetrahedron; and (5) discrepancies between the NMR results and crystal structure refinements for kyanite and wollastonite. These results indicate that both the Si–O bond length–chemical shift and bond strength–chemical shift relationships are useful tools for investigating the structures of crystalline silicates and, perhaps more importantly, silicate glasses, clays, and zeolites that cannot be examined by single crystal X-ray or neutron diffraction methods.

Introduction

High-resolution solid-state silicon-29 nuclear magnetic resonance spectroscopy is a powerful tool for investigating the structure and bonding properties of silicate crystals and glasses. In this paper we present data for the isotropic chemical shifts and chemical shift tensors of a wide range of natural and synthetic silicate crystals, and a correlation between the isotropic silicon-29 chemical shifts and the strength of the cation-oxygen bonds of the four oxygens coordinated to silicon. These results and interpretations are a first step in using NMR spectroscopy to interpret more fully the structures of less well understood materials, such as clays, fine grained zeolites, and glasses.

The first major investigation of solid-state silicon-29 NMR spectroscopy of inorganic materials was by Lippmaa *et al.* (1980, 1981), who found a correlation between chemical shift and extent of polymerization in silicate crystals. Since then, silicon-29 NMR has found signifi-

0003–004X/83/1112–1206$02.00

cant application in examining the structures of zeolite catalysts (Nagy *et al.*, 1981; Fyfe *et al.*, 1982; Thomas *et al.*, 1982; Klinowski *et al.*, 1982). Grimmer *et al.* (1981) have found an apparent correlation between chemical shift tensor element and Si–O bond length for axially symmetric silicon sites. Higgins and Woessner (1982) have proposed a correlation between isotropic chemical shift and average Si–O bond length in framework silicates.

The data presented here are for a much wider range of geologically important silicates than have been analyzed previously and are complementary to our oxygen-17, sodium-23, and aluminum-27 NMR studies of some of the same phases (Schramm *et al.* 1982, in press; Kinsey *et al*, 1982). Our silicon-29 work gives the main results listed in the abstract.

Theoretical background

A useful introduction to the NMR method is given in the book by Farrar and Becker (1971). Nevertheless, we wish to review briefly some of the theory here. Current high-resolution NMR techiques detect radiofrequency signals from nuclei which have been "excited" by resonant radiofrequency pulses. Each nuclide has a characteristic resonance frequency. The signals arise from transitions between nuclear energy levels. For a nucleus having a spin I there are (2I + 1) such energy levels, due to application of a static (Zeeman) magnetic field. The resonance frequency (ω_o) is directly proportional to the gyromagnetic ratio (γ) of the nucleus in question and the magnetic field (H_o):

$$\omega_o = \gamma H_o. \tag{1}$$

Because sensitive detection is obtained with the highest frequencies, H_o is chosen to be large. What makes the technique chemically useful is that the magnetic field, H_o, is modified by electronic effects in the material of interest, so that an "effective field", $H_o(1 - \sigma)$, modified by a screening constant, σ, is experienced by each nucleus. This results in a wide range of chemical shifts (or shieldings) of the resonance frequency for materials with different compositions and structures.

In polycrystalline solids at rest there are a number of phenomena which may broaden the NMR resonances, thus obscuring the chemically important information. These phenomena include an orientation-dependence of the chemical shift, magnetic dipole–dipole interactions between nuclei, and electric quadrupole interactions in which nuclei with quadrupole moments (spins I > 1/2) interact with electric field gradients in the chemical bonds. Silicon-29 has a spin I = 1/2 and thus does not suffer from such quadrupole broadening effects.

In liquids, rapid molecular tumbling causes a time-averaging of these static interactions, leading to narrow, well defined peaks, from which a great deal of structural information can be obtained. In non-rotating solids such rapid isotropic motion is absent. Time-averaging for solids can be obtained, however, by mechanically rotating the samples at rapid rates (typically ~2,500–5,500 Hz) in the magnetic field. A special angle, the so-called "magic-angle" (54.7° to the magnetic field, H_o), is used, because the linebroadening interactions contain ($3\cos^2\theta - 1$) terms in their time-dependent expansions (Andrew, 1971). At $\theta = 54.7°$, these terms for silicon-29 vanish, and narrow lines are obtained. In many solid phases magic-angle sample-spinning (MASS) reduces the peak width to about 1 ppm, allowing resoluton of chemical shifts almost as good as in liquid-state NMR.

In addition to a different isotropic chemical shift, the same nucleus in different materials may have a different chemical shift anisotropy (CSA), due to the fact that σ is a tensor quantity and reflects the three-dimensional nature of the electronic wavefunctions at each site. In MASS experiments this leads to so-called spinning side-bands, which are additional peaks on either side of the central one caused by modulation of the static interaction by sample rotation. The side-bands appear at multiples of the spinning frequency (ω_r) and change position and relative intensity with changing spinning rates. This makes it possible to identify them and to determine a variety of parameters related to the shielding (Herzfeld and Berger, 1980).

The NMR shielding parameters include the isotropic chemical shift σ_i (equal to one third of the trace of the shielding tensor, 1/3 Trσ); the principal values of the chemical shielding tensor, σ_{11}, σ_{22}, and σ_{33}; the shielding anisotropy (CSA), $\Delta\sigma$, which is defined as

$$\Delta\sigma = \sigma_{33} - 1/2(\sigma_{11} + \sigma_{22}); \tag{2}$$

and the asymmetry parameter, η, which is defined as

$$\eta = \frac{\sigma_{22} - \sigma_{11}}{\sigma_{33} - \sigma_i}. \tag{3}$$

In all of these expressions we use the convention

$$|\sigma_{33} - \sigma_i| \geq |\sigma_{11} - \sigma_i| \geq |\sigma_{22} - \sigma_i|, \tag{4}$$

which results in values of η from 0 to 1. The CSA is, thus, a measure of the magnitude of the overall spectral breadth for each silicon site and is related to chemical bonding, but in a complex manner which is as yet poorly understood for silicates.

It is, however, instructive to consider the bonding of, for example, carbon-13 in different chemical species. For example, for CH_2 groups in $(CH_2)_n$ (sp^3 bonds), $|\Delta\sigma|$ is ~31 ppm (Vanderhart, 1976), whereas for the CH_2 groups in ethylene (sp^2 bonds) $|\Delta\sigma|$ is 153 ppm (Zilm *et al.*, 1983). This is similar to the $|\Delta\sigma|$ of ~178 ppm to the sp^2 carbons in benzene (Linder *et al.*, 1979). For *sp* bonded carbon, $|\Delta\sigma|$ values are even larger (*e.g.*, 218 ppm for diacetylene, Cross and Waugh, 1977).

There are similar trends for $|\Delta\sigma|$ of silicon-29 in organosilicon species. For tetramesityldisilane, which has sp^3

bonds and silicons bonded to each other with single bonds, $|\Delta\sigma|$ is 25 ppm. For tetramesityldisilene, which has sp^2 bonds and silicons bonded to each other with double bonds, $|\Delta\sigma|$ is 119 ppm (Zilm *et al.*, 1983). Thus, the larger the differences in the types of chemical bond at a given carbon (or silicon), the larger the CSA. By contrast, the asymmetry parameter (η) is a measure of the departure of the chemical shielding tensor from *axial symmetry*. Thus, we might typically find $\eta = 0$ values for linear sp (diacetylene) or symmetric top sp^3 containing species, whereas aromatic sp^2 carbons might have $\eta \simeq 1$ reflecting a completely axially asymmetric electron distribution (Mehring, 1976). We comment briefly in this paper on the range of $\Delta\sigma$ and η values found in the silicates we have studied.

Experimental methods

Spectrometers

The spectra presented here were recorded on one of two "home-built" Fourier transform NMR spectrometers. One uses an 8.45 Tesla 3.5-inch bore high resolution superconducting solenoid (Oxford Instruments, Osney Mead, Oxford, England) together with a variety of digital and radiofrequency electronics, a Nicolet (Madison, WI) model 1180 computer, 293B pulse programmer, NIC-2090 dual channel transient recorder, and a Diablo model 40 disc system for data storage (Diablo Systems, Inc., Haywood, CA). The other system uses an 11.7 Tesla 2.0-inch bore solenoid (Oxford), and a Nicolet 1280 data system. Both instruments use Amplifier Research (Souderton, PA) model 200L amplifiers for final rf pulse generation, and are equipped with Andrew-Beams type magic-angle sample-spinning rotor assemblies (Andrew, 1971). At 8.45 Tesla (corresponding to a silicon-29 resonance frequency of 71.5 MHz) the sample volume is about 0.7 ml and rotation rates are from 1.0 to 3.0 kHz; at 11.7 Tesla (corresponding to a silicon-29 resonance frequency of 99.3 MHz) sample volume is about 0.2 ml and rotation rates are from 2.5 to 5.5 kHz. The 90° pulse widths at 8.45 Tesla are about 20 microseconds, and at 11.7 Tesla about 6 microseconds. The magic-angle was adjusted by optimizing the rotational echo train from a sample of V_2O_5. Chemical shifts are reported in ppm from external tetramethylsilane (TMS), taken as 6.6 ppm from hexamethyl disiloxane (in $Cr(acac)_3$ doped CH_2Cl_2). Larger negative chemical shifts (upfield shifts) indicate greater shielding.

Sample preparation

Most of the synthetic crystals were grown by crystallization at 50° to 100° below the solidus from melts of the same composition as the crystals. The melts were prepared by fusion in a Pt crucible three times with grinding in an agate mortar and pestle in between. Starting components were 99.999% pure SiO_2, MgO, Al_2O_3, and $CaCO_3$, and reagent grade Na_2CO_3, Li_2CO_3, K_2CO_3, $SrCO_3$, and $BaCO_3$. The synthetic montmorillionite was supplied by Professor D. Hendrickson of the University of Illinois School of Chemical Sciences. The forsterite, orthoenstatite, and clinoenstatite were supplied by Dr. A. Grandin de L'eprevire of the University of Illinois Department of Ceramics. The talc and pyrophyllite were provided by Professor J. Hower. The natural minerals are from the University of Illinois Mineralogical Collection. Localities are given in Table 1. Samples were generally ground to a fine powder using an agate (SiO_2) pestle and mortar before packing into the NMR rotor.

Sample characterization

All samples were characterized by powder X-ray diffractometry using a Norelco instrument (Mount Vernon, NY). The presence of magnetic impurities, which confound the extraction of CSA information from MASS NMR lineshapes (Oldfield *et al.*, 1983), was sought for in all samples by electron paramagnetic resonance (EPR) and magnetic susceptibility measurements. For all samples we recorded the 9 GHz electron paramagnetic resonance spectra at ~23°C, using a Varian (Palo Alto, CA) E-4 spectrometer, and the magnetic susceptibility, using a Cahn (Cerritos, CA) microbalance system, by means of the Faraday method.

Results and discussion

Table 1 presents the chemical shifts, chemical shift tensor elements, chemical shift anisotropies ($\Delta\sigma$), asymmetry parameters (η), and localities for the samples we have examined, together with results for a few critical samples examined by Lippmaa *et al.* (1980) and Grimmer *et al.* (1981).

Figures 1 and 2 present representative spectra for a variety of these phases. In all spectra except those of wollastonite, enstatite, and sodium disilicate the tall, central peaks are the centerband resonances, whereas any others are side-bands due to the CSA. For the three exceptions the true resonance is the first peak to the right of the tallest, as determined by varying the sample spinning speed and noting which peak does not move. All three of these phases have exceptionally high CSA. Quartz and pyrophyllite show essentially no side-bands, indicating very little CSA, whereas the others show significant CSA. CSA and side-band number and height cannot be directly correlated between spectra, however, because they also depend on field strength and spinning speed. These effects are taken into account in determining the parameters in Table 1. Spectra for other phases are available from one of the authors (RJK) on request.

Correlation of chemical shift and polymerization

Lippmaa *et al.* (1980) found a correlation between a higher field (more negative) chemical shift and increasing degree of silicate polymerization ($Q^0 \rightarrow Q^4$) and also found distinct ranges of chemical shifts for Q^0, Q^1, Q^2, Q^3, and Q^4 Si sites for those phases with no Al in the tetrahedral sites. The Q^n notation represents the number of bridging oxygens per Si tetrahedron. Lippmaa *et al.* also noted that as more phases were examined these ranges would probably overlap.

This latter prediction is indeed true. Figure 3 shows the ranges for each type of site including all data presently available. The overlaps range from none, for framework (Q^4) structures, to extensive, for monomer (Q^0) structures. It is clear that simple correlation of chemical shift and structure type for a phase of unknown structure is

Table 1. NMR parameters of silicates

Name	Formula	σ_i	σ_{11} σ_{22} σ_{33}	$\Delta\sigma$	η	Locality or Reference
			NESOSILICATES			
Forsterite	Mg_2SiO_4	-62	-90,-72,-24	57	0.47	Synthetic
Monticellite	$CaMgSiO_4$	-66	-44,-60,-94	-42	0.57	Synthetic
Andalusite	Al_2SiO_5	-80	-45,-78,-116	-54	0.17	Ogilby, CA
Kyanite	Al_2SiO_5	-83	-50,-79,-120	-56	0.89	Moores, PA
			SOROSILICATES			
Gehlenite	$Ca_2Al_2SiO_7$	-72	-122,-74,-20	78	0.92	Synthetic
Akermanite	$Ca_2MgSi_2O_7$	-73	-134,-84,-1	108	0.69	Synthetic
Lawsonite	$CaAl_2Si_2O_7(OH)\cdot H_2O$	-81	-123,-92,-28	80	0.58	Tiburon, CA
Tricalcium silicate hydrate (TCSH)	$Ca_6Si_2O_7(OH)_6$	-84	-109,-109,-35	64	0.0	Grimmer et al., 1981
Hemimorphite	$Zn_4(Si_2O_7)(OH)\cdot H_2O$	-80	NM			Unknown
			CYCLOSILICATES			
Potassium cyclotetra-silicate (KCTS)	$K_4H_4Si_4O_{12}$	-88	-63,-63,-141	-78	0.0	Lippmaa et al., 1980
Tetramethylammonium-silicate hydrate (TMAS)	$(Me_4N)_8Si_8O_{20}$	-99	-73,-73,-152	-79	0.0	Grimmer et al., 1981
			INOSILICATES			
Enstatite	$MgSiO_3$	-81 -83	-40,-70,-132 -41,-76,-133	-77 -74	0.59 0.70	Synthetic
Diopside	$CaMgSi_2O_6$	-84	-31,-73,-148	-96	0.66	Synthetic
Wollastonite	$CaSiO_3$	-89	-24,-85,-158	-104	0.88	Willsboro, NY
Strontium silicate	$SrSiO_3$	-85	-30 -71,-154	-104	0.59	Synthetic
Barium silicate	$BaSiO_3$	-80	-29 -71,-140	-90	0.70	Synthetic
Sillimanite	Al_2SiO_5	-87	-49,-83,-129	-63	0.81	Custer, SD
Tremolite	$Ca_2Mg_5Si_8O_{22}(OH)_2$	-91 -88	-107,-107,-59 -50,-77,-137	48 -74	0 0.55	Sheffield, MA
Spodumene	$LiAlSi_2O_6$	-92	-53,-81,-142	-75	0.56	New Mexico
			PHYLLOSILICATES			
Lithium disilicate	$Li_2Si_2O_5$	-93	-56,-72,-151	-87	0.12	Synthetic
Sodium disilicate	$Na_2Si_2O_5$	-95	-54,-70,-161	-99	0.24	Synthetic
Talc	$Mg_3Si_4O_{10}(OH)_2$	-98	NM	≈20	NM	Synthetic
Pyrophyllite	$Al_2Si_4O_{10}(OH)_2$	-95	NM	≈20	NM	Synthetic
Montmorillonite	$(Al,Mg)_8(Si_4O_{10})_3$ - $(OH)_{10}\cdot 12H_2O$	-93	NM	≈40	NM	Synthetic
Datolite	$CaBSiO_4(OH)$	-83	-43,-59,-147	-96	0.25	W. Patterson, NJ
			TECTOSILICATES			
Low Albite	$NaAlSi_3O_8$	-93,-97,-105	NM	0-20	NM	Amelia, VA
Microcline	$(K,Na)AlSi_3O_8$	-95,-97,-100	NM	0-20	NM	Middletown, CN
Anorthite	$CaAl_2Si_2O_8$	-83,-85,-90	NM	0-20	NM	Synthetic
Quartz	SiO_2	-108	NM	0-20	NM	Unknown
Danburite	$CaB_2Si_2O_8$	-89	NM	0	NM	Mexico

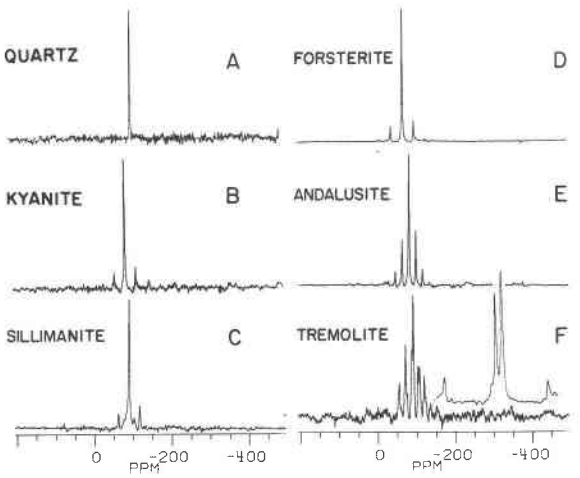

Fig. 1. 71.5 MHz ^{29}Si MASS NMR spectra of natural and synthetic minerals. A. Low quartz, 2.3 kHz MASS, 22 scans at 300 sec recycle time, 50 kHz spectral width, 27 μsec 90° pulse excitation, 2048 data points zero-filled to 8192, 100 Hz line-broadening due to exponential multiplication (Farrar and Becker, 1971). B. Kyanite (from Tyrol, Austria), 2.0 kHz MASS, 416 scans at 10 sec recycle time, 50 kHz spectral width, 28 μsec 90° pulse excitation, 2048 data points zero-filled to 8192, 100 Hz line-broadening. C. Sillimanite (from Brandywine Springs, PA), 2.0 kHz MASS, 368 scans at 1 sec recycle time, 50 kHz spectral width, 28 μsec 90° pulse excitation, 2048 data points zero-filled to 8192, 100 Hz line-broadening. D. Synthetic forsterite, 2.1 kHz MASS, 5952 scans at 10 sec recycle time, 50 kHz spectral width, 5.4 μsec 23° pulse excitation, 2048 data points zero-filled to 8192, 100 Hz line-broadening. E. Andalusite (from Oligby, CA), 1.2 kHz MASS, 472 scans at 1 sec recycle time, 50 kHz spectral width, 21 μsec 90° pulse excitation, 2048 data points zero-filled to 8192, 100 Hz line-broadening. F. Tremolite (from Sheffield, MA), 1.1 kHz MASS, 336 scans at 1 sec recycle time, 50 kHz spectral width, 20 μsec 90° pulse excitation, 2048 data points zero-filled to 8192, 100 Hz line broadening due to exponential multiplication. Inset: 99.3 MHz, 3.4 kHz MASS, 504 scans at 5 sec recycle time, 9 kHz spectral width, 6 μsec 90° pulse excitation, 4096 data points zero-filled to 8192, 50 Hz line-broadening, expanded plot.

likely to be risky, although the chemical shift parameter can probably be used as a guide as to the structure(s) present.

Correlation of isotropic chemical shift, Si–O bond length, and cation–oxygen bond strength

In order to find a more comprehensive way of understanding the effect of polymerization state on chemical shift, the overlap between ranges of different polymer types, and the lower field (less negative) shifts of phases with tetrahedrally coordinated Al (Lippmaa *et al.*, 1981), and to aid in interpretation of spectra for phases with poorly known structures, we have attempted to find correlations of the isotropic chemical shift with average Si–O bond lengths and with cation-oxygen bond strengths using the Brown and Shannon (1973) values. Table 2 presents the data for those phases for which high quality structure refinements are available.

Figure 4 shows that the correlation between average Si–O bond length and isotropic chemical shift is poor, especially for the chain silicates, which have chemical shifts between −80 and −90 ppm. Many sites fall significantly off the least squares line, which has a correlation coefficient of 0.84.

Because the Si sites in all phases examined here are 4-coordinated by oxygen, it seems likely that much of the scatter in the chemical shift *versus* Si–O bond length diagram is due to next-nearest neighbor (NNN) interactions. Because a rigorous quantum mechanical treatment of the chemical shift in silicates is lacking, we have chosen to treat the effect of the NNN atoms by using the

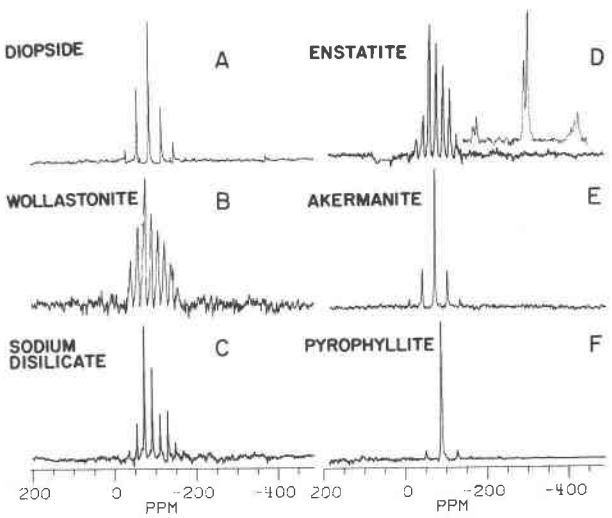

Fig. 2. 71.5 MHz ^{29}Si MASS NMR spectra of natural and synthetic minerals. A. Synthetic diopside crystals, 2.1 kHz MASS, 248 scans at 10 sec recycle time, 50 kHz spectral width, 5.4 μsec 23° pulse excitation, 2048 data points zero-filled to 8192, 100 Hz line-broadening due to exponential multiplication. B. Wollastonite, 1.2 kHz MASS, 376 scans at 120 sec recycle time, 50 kHz spectral width, 21 μsec 90° pulse excitation, 2048 data points zero-filled to 4096, 100 Hz line-broadening. C. Sodium disilicate ($Na_2Si_2O_5$), 1.3 kHz MASS, 183 scans at 300 sec recycle time, 50 kHz spectral width, 27 μsec 90° pulse excitation, 2048 data points zero-filled to 8192, 100 Hz line-broadening. D. Synthetic enstatite crystals, 1.2 kHz MASS, 385 scans at 60 sec recycle time, 50 kHz spectral width, 28 μsec 90° pulse excitation, 2048 data points zero-filled to 4096, 100 Hz line broadening due to exponential multiplication. Inset: 99.3 MHz, 3.4 kHz MASS, 250 scans at 10 sec recycle time. 9 kHz spectral width, 3.5 μsec 53° pulse, 4096 data points zero-filled to 8192, 50 Hz line-broadening, expanded plot. E. Synthetic akermanite crystals, 2.1 kHz MASS, 1700 scans at 10 sec recycle time, 50 kHz spectral width, 2.6 μs 23° pulse excitation, 2048 data points zero-filled to 8192, 100 Hz line-broadening. F. Pyrophyllite, 2.7 kHz MASS, 21 scans at 600 sec recycle time, 50 kHz spectral width, 30 μsec 90° pulse excitation, 2048 data points zero-filled to filled to 8192, 100 Hz line-broadening.

bond strengths of Brown and Shannon (1973). These bond strengths are similar to the electrostatic bond strengths of Pauling (1939), but are modified empirically to include the effect of interatomic distance. To do this we total the cation-oxygen bond strengths for all cations bonded to the four oxygens of the tetrahedron. This includes the Si atom itself and all cations outside the tetrahedron which are coordinated to these oxygens.

Pauling's original postulate was that the sum of the electrostatic bond strengths of the cations surrounding an oxygen atom should equal the absolute value of the valence of oxygen, where the bond strength from a cation is its valence divided by its coordination number. This "Pauling's second rule" has been used ever since in evaluating crystal structures determined by X-ray and neutron diffraction. Work since then (*e.g.*, Baur, 1978; Brown and Shannon, 1973) has shown that the rule does not hold exactly for many structures, and that bond lengths increase or decrease to compensate for too much or too little charge.

Figure 5 presents the relationship between ^{29}Si chemical shift and total cation–oxygen bond strength (in valence units) for the four oxygens coordinating each Si site. All points in Figure 5 fall within ±2% of the best fit line, and most fall within ±1%. This is well within the ±4% error in the bond strengths given by Brown and Shannon, and probably reflects the overall better quality of the structure refinements we have used. The correlation coefficient of the line is 0.93.

The bond strength–chemical shift correlation would appear to be somewhat more useful than the bond length–chemical shift correlation, because all points fall within the error limits and because it takes into account more of the crystal structure. Both correlations generally give the same site assignments for different peaks in the same phase. The bond strength correlation also brings the orthosilicates closer to the best fit line, whereas many of them fall significantly to the right in the bond length correlation.

The bond strength-chemical shift relationship in Figure 5 offers an explanation of the ranges of chemical shifts for different structural types observed by Lippmaa *et al.* (1980), for the overlap of these ranges in Figure 1, and for the deshielding caused by Al substitution in the Si sites.

The bond strength sums for a particular structure type tend to fall into one range because the average number of Si atoms bonded to a tetrahedron decreases with decreased polymerization. Silicon atoms have the largest effect because the Si–O bond is the strongest one involved (443 kJ/gram atom, Kingery *et al.*, 1976). Variation in the kind and arrangement of other cations within a given structure type, however, causes the ranges in chemical shift to be large enough to overlap. This is especially true if there is Al in 6-fold coordination, as in the aluminosilicate polymorphs. Al substitution for Si in the 4-fold sites results in a lower bond strength sum

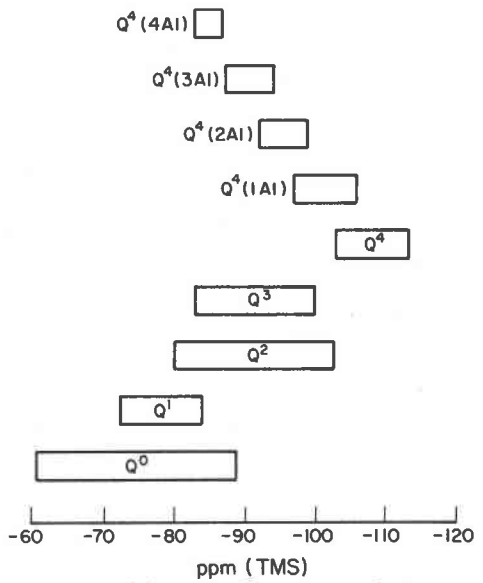

Fig. 3. Ranges of isotropic chemical shifts for silicon sites with different polymerizations for phases with Si in tetrahedral coordination.

because the Al–O bond is weaker (330–422 kJ/gram atom) than the Si–O bond, which correlates with a less negative chemical shift.

The relationships of both the Si–O bond length and bond strength with chemical shift are useful for examining the structures of crystalline silicates and, perhaps more importantly, silicate glasses, clays, and fine grained zeolites whose structures cannot be determined by single crystal X-ray or neutron diffraction methods. Proposed structures for materials with known NMR behavior must have the correct number of crystallographically distinct Si sites, Si–O bond lengths consistent with Figure 4, and cation-oxygen bond strengths consistent with Figure 5.

Chemical shift anisotropy and asymmetry parameter.

Although both the CSA and asymmetry parameter must reflect in some way the crystal structure and bonding, the relationships are less well understood than for the isotropic chemical shift. Interpretation of CSA data of natural minerals may be complicated by the presence of paramagnetic atoms, either in the crystal structure or in a finely dispersed separate phase, which may add a spurious contribution to the CSA (Oldfield *et al.*, 1983). None of the samples listed in Table 1 have a significant EPR signal or magnetic susceptibility, which might indicate an appreciable anomalous CSA.

The framework silicates, hydrous sheet silicates, and hemimorphite all have small CSA's and anisotropy pa-

Table 2. Isotropic chemical shifts, Si–O bond length and cation–oxygen bond strengths for phases with well-known structures

		^{29}Si CHEMICAL SHIFT (PPM - TMS)	MEAN Si–O BOND LENGTH (Å)	TOTAL CATION-OXYGEN BOND STRENGTH (VALENCE UNITS)	REFERENCE
			NESOSILICATES		
Forsterite (1)		- 62	1.637(2)	7.721	Brown, 1980, Rev. Min., 5, 275.
Monticellite (2)		- 66	1.641(1)	7.689	Brown, 1980, Rev. Min., 5, 275.
Andalusite (3)		- 80	1.631(3)	8.034	Winter and Ghose, 1979, Am. Min., 64, 573.
Kyanite (4)	Si(1)	- 83	1.635(2)	7.978	Winter and Ghose, 1979, Am. Min., 64, 573.
	Si(2)	- 83	1.636(2)	7.939	
			SOROSILICATES		
Lawsonite (5)		- 81	1.633(2)	- [1]	Bauer, 1978, Am. Min., 63, 311.
Hemimorphite (6)		- 80	1.623(2)	8.061[1]	Hill et al., 1977, Zeit. Krist., 146, 241.
			INOSILICATES		
Enstatite (7)	SiA	- 84	1.628(2)	8.188	Ohaski and Finger, 1976, Carnegie Inst., Wash. Yearbook, 75, 743.
	SiB	- 81	1.638(2)	7.943	
Diopside (8)		- 85	1.634(2)	8.077	Clark et al., 1969, Min. Soc. Am. Spec. Pap. 2, 33.
Wollastonite (9)	Si(1)	- 89	1.624(5)	7.926	Peacor and Prewitt, 1963, Am. Min., 48, 588.
	Si(2)		1.621(5)	7.989	
	Si(3)		1.634(5)	8.110	
$BaSiO_3$ (10)		- 80	1.623(3)	Bond Strength Not Calculated	Grosse and Tillmanns, 1974, Cryst. Struct. Comm., 3, 603.
Sillimanite (11)		- 87	1.627(2)	8.101	Winter and Ghose, 1979, Am. Min., 64,573.
Tremolite (12)	T(1) Q_3 Site	- 91	1.620(2)	8.253	Papike et al., 1969, Min. Soc. Am. Spec. Paper 2, 117.
	T(2) Q_2 Site	- 88	1.632(2)	8.015	
Spodumene (13)		- 91	1.618(2)	8.279	Clark et al., 1969, Min. Soc. Am. Spec. Paper, 2, 31.
			PHYLLOSILICATES		
$Na_2Si_2O_5$ (14)		- 95	1.617(4)	8.225	Pant and Cruickshank, 1968, Acta. Cryst. Cryst., B24, 13.
Datolite (15)		- 83	1.642(5)	8.052	Pant and Cruickshank, 1967, Zeit. Krist. 125, 286.
			TECTOSILICATES		
Low Albite (16)	T_1M	-105	1.609(1)	8.379	Harlow and Brown, 1980, Am. Min., 65, 986.
	T_1O	- 97	1.614(1)	8.367	
	T_2M	- 93	1.616(1)	8.238	
Microcline (17)	T_1M	-100	1.614(5)	8.394	Brown and Bailey, 1964, Acta Cryst., 17, 1391.
	T_2M	- 97	1.612(5)	8.348	
	T_2O	- 95	1.611(5)	8.310	
Cristobalite (18)		-110[2]	1.605(2)	8.468	Dollase, 1965, Zeit. Krist., 121, 369.
Quartz (19)		-108	1.609(1)	8.364	LePage and Donnay, 1976, Acta Cryst., B32, 2456.
Natrolite (20)	T(1)	- 96	1.617(4)	- [1]	Peacor, Am. Min., 1973, 58, 676.
	T(2)	- 88	1.621(4)	-	

[1]Total bond strengths for structures with bound H_2O have not been calculated unless a neutron diffraction refinement is available.
[2]Chemical shifts not listed in Table 1 are from Lippmaa et al., 1980.

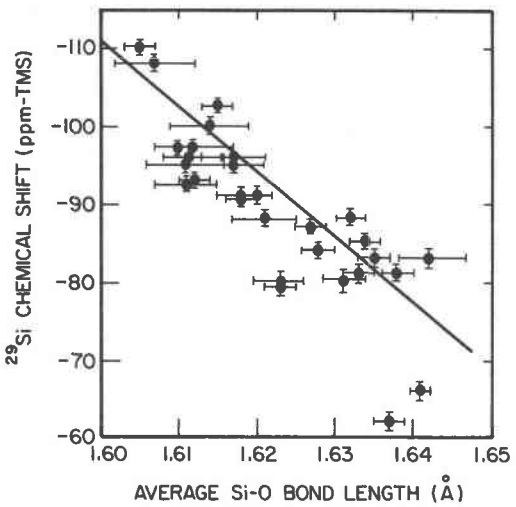

Fig. 4. Silicon-29 solid state isotropic chemical shift *versus* average Si–O bond length. Note that many ino- and sorosilicates fall significantly off the trend.

rameters too small to measure. This implies a relatively symmetric electron distribution around Si. The anhydrous sheet silicates, the cyclosilicates, datolite, the Q_3 site of tremolite, TCSH, and andalusite have moderate to large CSA's but small asymmetry parameters, indicating essentially axial symmetry of the electron distribution around Si.The remaining phases, most of the nesosilicates, sorosilicates, and chain silicates, have moderate to large CSA's and asymmetry parameters, indicating a significantly non-symmetric electron distribution around Si. Grimmer *et al.* (1981) have proposed that sorosilicates should have axial symmetry. Our data show, perhaps surprisingly, that this need not be the general rule.

Our observations show that CSA and asymmetry parameters are roughly correlated with composition and structure. We have not yet, however, been able to correlate them quantitatively with any parameter related to bond length or bond strength. Further work is required to make use of these NMR parameters in obtaining structural data on silicates.

NMR observation of phases with multiple Si sites

Any phase in which all Si sites are crystallographically equivalent should exhibit a single silicon-29 NMR peak. Our results are all consistent with this idea. Phases having non-equivalent silicon sites should exhibit as many peaks as there are sites, each caused by slightly different environments around each type of site. Our results for such phases, however, are not wholly consistent with the X-ray diffraction results, even though our instruments are capable of resolving differences in isotropic chemical shifts at least as small as 1 ppm.

Enstatite, tremolite and low albite (Table 2), on the one hand, have multiple peaks, each corresponding to a particular type of silicon site. The expanded-scale spectra in Figures 1F and 2D clearly show these peaks for pairs of non-equivalent silicon sites in tremolite and enstatite. The non-equivalent silicon sites in these minerals have differences in bond strength sums of about 0.25 valence units and differences in chemical shift of about 3 ppm (Table 2). Low albite has three non-equivalent sites and exhibits three well-resolved peaks. Adjacent chemical shifts differ by 4 and 8 ppm; the corresponding differences in sum of Si–O bond strengths are only 0.13 and 0.01 (Table 2).

On the other hand, kyanite and wollastonite also have crystallographically non-equivalent silicon sites but show only one peak (Table 2), even in expanded scale spectra. The single peak for kyanite (Fig. 1B) is as sharp as that for a phase having only one silicon site. The peak for wollastonite (Fig. 2B) is not quite as narrow but shows no detectable splitting.

At this time we cannot offer a wholly satisfactory explanation for the lack of multiple peaks in kyanite and wollastonite. According to the X-ray structure refinements available to us (Table 2): (1) the difference in bond strength sum between sites Si(1) and Si(2) in kyanite is 0.04, and (2) the differences between sites Si(1) and Si(2) and between sites Si(2) and Si(3) in wollastonite are 0.06 and 0.12, respectively. Although these are smaller differences than in enstatite and tremolite, they are no smaller than those of low albite. It is possible that the X-ray refinements of the structures of kyanite and wollastonite are slightly in error and that the environments around the non-equivalent silicon site of each structure actually differ even less from one another than is indicated in Table 2.

In any case, even though there is a relatively good correlation between chemical shift and bond strength sum, it is unlikely that this is the only factor affecting chemical shift. Further work is needed.

Effect of paramagnetic impurities

In addition to the data presented above, we have also attempted to investigate several natural paramagnetic

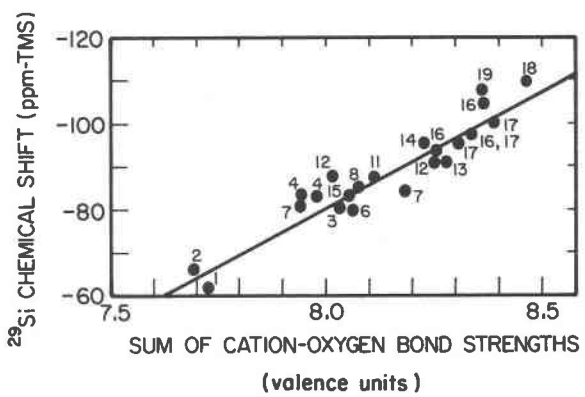

Fig. 5. Silicon-29 isotropic chemical shift *versus* total cation-oxygen bond strength for the four oxygen atoms surrounding each Si site. Numbers correspond to designation in Table 2.

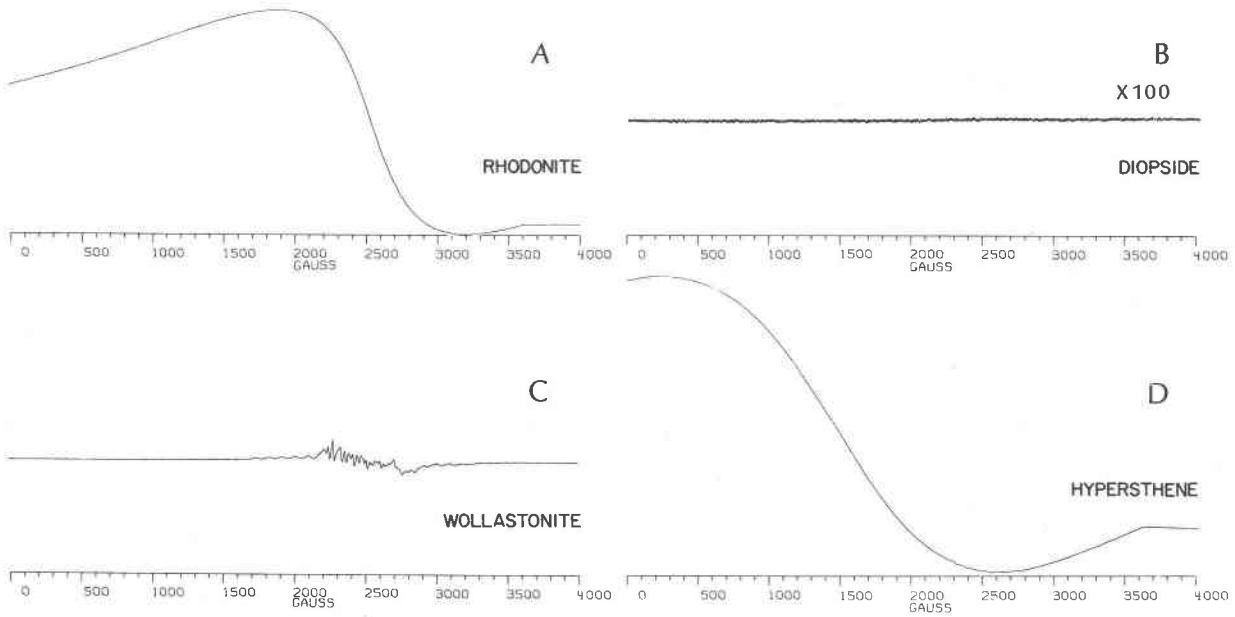

Fig. 6. 9 GHz EPR spectra of: (A) rhodonite ($MnSiO_3$); (B) diopside ($CaMgSi_2O_6$); (C) wollastonite ($CaSiO_3$); (D) hypersthene ($(Mg,Fe)SiO_3$). All spectra obtained at approximately 23°C, under identical instrumental conditions, except that the vertical gain in (B) is 100 times that of the other spectra.

phases, including hypersthene, ($(Mg,Fe)SiO_3$), rhodonite ($MnSiO_3$), jadeite (ideal formula, $NaAlSi_2O_6$), and actinolite, ($Ca_2(Mg,Fe)_5Si_8O_{22}(OH)_2$). Unfortunately, rhodonite does not spin rapidly in our 8.45 Tesla field (presumably because of its large paramagnetism), and no signal was seen from the other phases. This is due, we believe, to extensive linebroadening and sideband formation caused by paramagnetic ions present, or in some cases to ferromagnetic or antiferromagnetic inclusions (Oldfield *et al.*, 1983).

This inability to observe silicon-29 NMR signals correlates well with the ability to readily observe high signal-to-noise ratio EPR signals. Figure 6 presents the 9 GHz EPR spectra of rhodonite, hypersthene, wollastonite, and synthetic diopside. For rhodonite there is a broad resonance centered around a g-value of 2. This arises from the strong exchange coupling between the d^5 Mn^{2+} ions and correlates with a large magnetic susceptibility. Similar results were obtained for hypersthene, whose EPR spectrum displays an intense exchange-broadened resonance due to Fe^{2+}. For wollastonite the EPR spectrum is characteristic of a dilute Mn^{2+} ion, with some additional hyperfine structure. The magnetic susceptibility of this sample is approximately 1% that of rhodonite and hypersthene, and is close to the noise level of our measurements, consistent with a well-resolved silicon-29 NMR spectrum (Fig. 1). For diopside, there is essentially no EPR absorption, in agreement with an observed magnetic susceptibility of approximately zero. The EPR results for all of the other synthetic materials produced in our laboratories are similar to those for diopside.

Acknowledgments

We wish to thank the people who supplied us with some of the samples, and Robert A. Kinsey and Suzanne E. Schramm for much useful discussion. This work was supported in part by the U.S. National Science Foundation (grants EAR79-03923, PCM79-23170, PCM81-17813, EAR82-07260), the U.S. National Institutes of Health (grant HL-19481) and the American Heart Association (AHA80-867), and has benefitted from facilities provided by the University of Illinois—National Science Foundation Regional NMR Instrumentation Facility (grant CHE79-16100). E. O. is a USPHS Research Career Development Awardee, 1979–1984. A review by James B. Murdoch significantly improved the original version.

References

Andrew, E. R. (1971) The narrowing of NMR spectra of solids by high-speed specimen rotation and the resolution of chemical shift and spin multiplet structures for solids. Progress in NMR spectroscopy, 8, 1–39.

Baur, W. H. (1978) Variation of mean Si–O bond lengths in silicon–oxygen tetrahedra. Acta Crystallographica, B34, 1751–1756.

Brown, I. D. and Shannon, R. D. (1973) Empirical bond-strength–bond-length curves for oxides. Acta Crystallographica, A29, 266–282.

Cross, V. R. and Waugh, J. S. (1977) ^{13}C chemical shift anisotropy and CH bond length in diacetylene. Journal of Magnetic Resonance, 25, 225.

Farrar, T. C. and Becker, E. D. (1971) Pulse and Fourier Transform NMR: Introduction to Theory and Methods. Academic Press, New York.

Fyfe, C. A., Gobbi, G. C., Klinowski, J., Thomas, J. M., and Ramdas, S. (1982) Resolving crystallographically distinct tet-

rahedral sites in silicalite and ZSM-5 by solid-state NMR. Nature, 296, 530–536.

Grimmer, A.-R., Peter, R., Fechner, E., and Molgedey, G. (1981) High-resolution ^{29}Si NMR in solid silicates. Correlations between shielding tensor and Si–O bond length. Chemical Physics Letters, 77, 331–335.

Herzfeld, J. and Berger, A. E. (1980) Sideband intensities in NMR spectra of samples spinning at the magic angle. Journal of Chemical Physics, 73, 6021–6030.

Higgins, J. B. and Woessner, D. E. (1982) ^{29}Si, ^{27}Al, and ^{23}Na spectra of framework silicates. (abstr.) Transactions of the American Geophysical Union (EOS), 63, 1139.

Kingery, W. D., Bowen, H. K., and Uhlmann, D. R. (1976) Introduction to Ceramics. Wiley and Sons, New York.

Kinsey, R. A., Smith, K. A., Oldfield, E., Kirkpatrick, R. J., and Hower, J. (1982) Applications of high-resolution NMR spectroscopy to silicates. (abstr.) Transactions of the American Geophysical Union (EOS), 63, 1139.

Klinowski, J., Ramdas, S., Thomas, J. M., Fyfe, C. A. and Hartman, J. S. (1982) A re-examination of Si, Al ordering in zeolites NaX and NaY. Journal of the Chemical Society, Faraday Transactions II, 78, 1025–1050.

Linder, M., Höhener, A., and Ernst, R. R. (1979) Proton-enhanced carbon-13 resonance in helium cooled probe; chemical shielding tensor of benzene. Journal of Magnetic Resonance, 35, 379–386.

Lippmaa, E., Mägi, M., Samoson, A., Engelhardt, G., and Grimmer, A.-R. (1980) Structural studies of silicates by solid-state high-resolution ^{29}Si NMR. Journal of the American Chemical Society, 102, 4889–4893.

Lippmaa, E., Mägi, M., Samoson, A., Tarmak, M., and Engelhardt, G. (1981) Investigation of the structure of zeolites by solid-state high-resolution ^{29}Si NMR spectroscopy. Journal of the American Chemical Society, 103, 4992–4996.

Mehring, M. (1976) High-resolution NMR spectroscopy in solids. Springer-Verlag, New York.

Nagy, J. B., Gilson, J.-P., and Derouane, E. G. (1981) Evidence for secondary building unit effects on the solid state ^{29}Si NMR resonance of silicon in zeolite structures. Journal of the Chemical Society, Chemical Communications, 1129–1131.

Oldfield, E., Kinsey, R. A., Smith, K. A., Nichols, J. A., and Kirkpatrick, R. J. (1983) High-resolution NMR of inorganic solids. Influence of magnetic centers on magic-angle sample-spinning lineshapes in some natural aluminosilicates. Journal of Magnetic Resonance, 51, 325–329.

Pauling, L. (1939) The Nature of the Chemical Bond, 1st Edition. Cornell University Press, Ithaca, New York.

Schramm, S., Kirkpatrick, R. J., and Oldfield, E. (1982) Observation of high-resolution ^{17}O NMR spectra of inorganic solids. Journal of the American Chemical Society, 105, 2483–2485.

Thomas, J. M., Fyfe, C. A., Ramdas, S., Klinowski, J., Gobbi, G. E. (1982) High-resolution silicon-29 nuclear magnetic resonance spectrum of zeolite ZK-4: Its significance in assessing magic-angle-spinning nuclear magnetic resonance as a structural tool for aluminosilicates. Journal of Physical Chemistry, 86, 3061–3064.

Vanderhart, D. L. (1976) Characterization of the methylene ^{13}C chemical shift tensor in the normal alkane n-$C_{20}H_{42}$. Journal of Chemical Physics, 64, 830–834.

Zilm, K. W., Grant, D. M., Michl, J., Fink, M. J. and West, R. (1983) Electronic structure of the silicon-silicon double bond. Silicon-29 shielding anisotropy in tetramesityldisilene. Organometallics, 2, 193–194.

Manuscript received, December 29, 1982;
accepted for publication, May 2, 1983.

Note Added in Proof

J. V. Smith and C. S. Blackwell (Nature, 303, 223, 1983) have presented a linear relationship between the silicon-29 chemical shift and the mean secant of the Si–O–Si bond angle for the SiO_2 polymorphs. We have also become aware of an unpublished X-ray refinement of maximum microcline that may change the site assignments in Table 2.